

Enhanced hybridization sets the stage for electronic nematicity in CeRhIn₅

P. F. S. Rosa¹, S. M. Thomas¹, F. F. Balakirev², E. D. Bauer¹,

R. M. Fernandes³, J. D. Thompson¹, F. Ronning¹, and M. Jaime²

¹ *Los Alamos National Laboratory, Los Alamos, New Mexico 87545, U.S.A.*

² *National High Magnetic Field Laboratory, Los Alamos, New Mexico 87545, U.S.A.*

³ *School of Physics and Astronomy, University of Minnesota, Minneapolis, Minnesota 55455, USA.*

(Dated: March 16, 2022)

High magnetic fields induce a pronounced in-plane electronic anisotropy in the tetragonal anti-ferromagnetic metal CeRhIn₅ at $H^* \gtrsim 30$ T for fields $\simeq 20^\circ$ off the c -axis. Here we investigate the response of the underlying crystal lattice in magnetic fields to 45 T via high-resolution dilatometry. Within the antiferromagnetic phase of CeRhIn₅, a finite magnetic field component in the tetragonal ab -plane explicitly breaks the tetragonal (C_4) symmetry of the lattice well below H^* revealing a finite nematic susceptibility at low fields. A modest magnetostriction anomaly, $dL/L = -1.8 \times 10^{-6}$, at $H^* = 31$ T hence presumably marks the crossover to a fluctuating nematic phase with large electronic nematic susceptibility. Magnetostriction quantum oscillations confirm a Fermi surface change at H^* with the emergence of new orbits. By analyzing the field-induced change in the crystal-field ground state, we conclude that the in-plane Ce $4f$ hybridization is enhanced at H^* , carrying the in-plane f -electron anisotropy to the Fermi surface. We argue that the nematic behavior observed in this prototypical heavy-fermion material is of electronic origin, and is driven by the hybridization between $4f$ and conduction electrons.

For more than half a century, the investigation of rare-earth-based materials has provided predictive understanding in both fundamental and applied realms [1]. From the quantum theory of magnetism to the design of magnets in hard-drives, these materials, synthesized with $4f$ open-shell elements, have stimulated a diverse set of scientific discoveries. Cerium-based materials are a particularly intriguing case because their $4f$ electron may hybridize with the sea of conduction electrons [2]. The f -electron delocalization destabilizes the otherwise magnetically ordered ground state and novel quantum phenomena may arise at the Fermi surface (FS).

Heavy electron masses, unconventional superconductivity, and non-Fermi-liquid behavior are a few known examples of emergent phenomena in Ce-based materials [3]. More recently, the discovery of a large electronic in-plane anisotropy induced by high magnetic fields in tetragonal CeRhIn₅ reveals the possibility of yet another novel state of matter, the so-called XY nematic [4]. In an electronic nematic phase, the symmetry of the electronic system is lowered compared to that of the underlying lattice, in analogy to the directional alignment in nematic liquid crystals with continuous translational symmetry [5, 6]. Above an out-of-plane critical field of $H^* \approx 30$ T, but within the antiferromagnetic (AFM) phase, electrical resistivity measurements reveal electronic nematicity in CeRhIn₅. The small in-plane field component necessary to break the rotational symmetry of the electronic structure suggests a remarkably large nematic susceptibility. Moreover, the small magnitude of the magnetostriction anomaly at H^* , along with a similar response in the B_{1g} and B_{2g} channels, indicates that this phase is not strongly pinned to the lattice, placing CeRhIn₅ as a rare XY-nematic candidate. At H^* , torque magnetometry measurements also identify a FS reconstruction and point to a larger FS in the nematic phase [7, 8].

At zero field and zero pressure, CeRhIn₅ undergoes a phase transition to a helix AFM order at $T_N = 3.8$ K with ordering wavevector $\mathbf{Q}_1 = (0.5, 0.5, 0.297)$ [9–11]. Pressurizing CeRhIn₅ tunes T_N toward a quantum-critical point (QCP) at $P_{c2} = 2.3$ GPa and induces unconventional superconductivity around it [12–14]. At P_{c2} the effective electron mass diverges and the FS changes abruptly [15]. Applied pressure is a clean tuning parameter known to increase the hybridization between $4f$ and conduction electrons, and, as a consequence, the T - P phase diagram of CeRhIn₅ can be qualitatively understood in terms of the strength of the (Kondo) coupling between $4f$ and conduction electrons [16]. Remarkably, magnetic fields also destabilize the AFM order in CeRhIn₅ towards a QCP at $H_c \approx 50$ T and a FS reconstruction is observed at $H^* \approx 30$ T [7]. Magnetic fields, however, are symmetry breaking and expected to localize $4f$ electrons. Understanding why the Kondo coupling is robust in high fields is a first step towards unveiling the nature of the nematic phase. An additional relevant question is whether the H^* boundary is a true (first-order) phase transition or a crossover.

To answer these questions, probes other than electrical resistivity are imperative. Various thermodynamic probes such as torque magnetometry, magnetic susceptibility, and specific heat, however, fail to observe an anomaly at H^* , although their response is affected above it. Apart from the FS reconstruction seen by magnetometry, specific heat measurements in pulsed fields show a clear difference in the shape of the peak at T_N across H^* [17]. In this Letter, we use high-resolution dilatometry to probe the response of the underlying crystal lattice to magnetic fields. The finite coupling between the nematic phase and the lattice yields an anomaly at H^* that can be tracked to high temperatures and vanishes above the AFM boundary. A finite in-plane field component ex-

explicitly breaks the tetragonal (C_4) symmetry of the lattice revealing a finite nematic susceptibility at low fields. The small magnetostriction anomaly at $H^* = 31$ T hence marks the crossover to a fluctuating nematic phase with large nematic susceptibility. This crossover occurs concomitantly to a Fermi surface change at H^* and an enhancement in the Ce $4f$ hybridization with the in-plane In(1) conduction electrons, suggesting that the nematic phase stems from the $4f$ degrees of freedom and their anisotropy which is translated to the Fermi surface via hybridization. The Fermi surface change is confirmed by unprecedented quantum oscillations in the magnetostriction of CeRhIn₅ that reveal the emergence of new orbits.

Single crystals of CeRhIn₅ were grown by the Indium-flux technique. The crystallographic structure and orientation were verified by X-ray powder diffraction and Laue diffraction at 300 K, respectively. Low-field magnetostriction measurements were performed using the standard capacitance dilatometry technique in a Quantum Design PPMS above 2 K [18]. The longitudinal and transverse magnetostriction of CeRhIn₅ was obtained as a function of DC fields to 9 T applied parallel to the a -axis with a resolution in dL/L of 10^{-8} . High-field magnetostriction measurements were performed using optical Fiber Bragg Grating (FBG) sensors in a hybrid magnet at ^3He temperatures [19]. The c -axis magnetostriction, dL_c/L_c , was obtained as a function of DC fields to 45 T applied $\simeq 20^\circ$ off the c -axis. The data was obtained with a swept wavelength laser Micron Optics interrogator, yielding a resolution of 3×10^{-8} .

The first point we will address is how the system responds to an in-plane magnetic field that explicitly breaks tetragonal symmetry. Figure 1 shows the anisotropic magnetostriction of CeRhIn₅ for fields applied along the a -axis. When $dL||H||a$, the longitudinal magnetostriction is negative and displays a sharp contraction at 2.2 T, signaling the transition from a helix state (AF1) to a commensurate collinear square-wave state (AF3) with ordering vector $\mathbf{Q}_3 = (1/2, 1/2, 1/4)$ [11]. The transverse magnetostriction ($dL||b$), however, is positive and displays a sharp expansion at 2.2 T. In a conventional material, compression along the a -axis produces an expansion along the perpendicular axes (i.e. b - and c -axes), and the ratio of the perpendicular strains is known as the Poisson's ratio, ν_{ij} [20]. In particular, ν_{xy} gives the in-plane strain response. The calculated Poisson's ratio in this scenario is $\nu_{xy} \equiv s_{xy}/s_{xx} = 0.2$, where s_{ij} are the elastic compliances at 10 K obtained from the inverted elastic modulus tensor [21]. The experimental ratio between the transverse and longitudinal magnetostriction response, however, is not only larger than the calculated one, but also field- and temperature-dependent. This difference suggests that there are other degrees of freedom contributing to the observed response.

To describe these observations and model the magneto-elastic coupling in this material, we write the magneto-elastic free energy of a tetragonal system as $F = -\lambda\delta(H_a^2 - H_b^2) + (\alpha/2)\delta^2$, where $\delta = (a - b)/a$

is the orthorhombic distortion, λ is a coupling constant, and α is the elastic constant renormalized by nematic fluctuations acting as an indirect measure of the nematic susceptibility. As a consequence, one can estimate the nematic susceptibility, χ_{nem} , from the data via $\chi_{\text{nem}} \propto \partial\delta/\partial H_a^2$, where $\delta = dL_a/L_a - dL_b/L_b$. Our results show that $\gamma\chi_{\text{nem}} = -2 \times 10^{-9}$ in the AF1 phase and $\gamma\chi_{\text{nem}} = -6 \times 10^{-10}$ in the AF3 phase. The nematic susceptibility is finite, but curiously smaller in AF3. This result suggests that χ_{nem} is small in the low field phases and is not enhanced as a function of magnetic fields. In fact, the nematic response in the electronic degrees of freedom, i.e., the in-plane resistivity anisotropy, is vanishingly small at low fields and increases sharply at H^* (inset of Fig. 1). We note that the nematic order parameter couples to any quantity that breaks tetragonal symmetry. As a consequence, nematic fluctuations – and hence the corresponding nematic susceptibility – can be indirectly probed in different quantities, such as the elastic constant α or the rate of change of the anisotropic resistivity, with different coupling strengths.

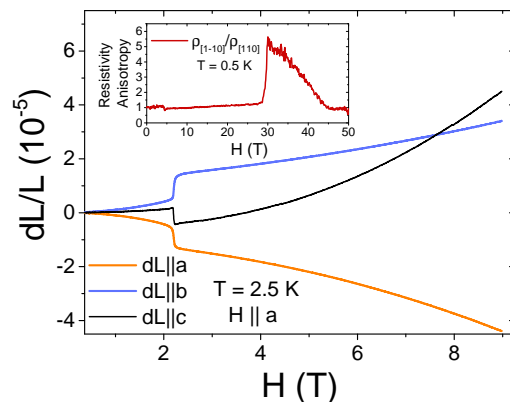


FIG. 1. Magnetostriction of CeRhIn₅ along the a -axis, dL_a/L_a , at 2.5 K for fields applied in the tetragonal ab -plane. Inset shows the in-plane anisotropy in electrical resistivity [4].

Next, we turn our attention to the lattice response at fields applied 20° off the c -axis at which the in-plane resistivity anisotropy is pronounced. Figure 2 shows the c -axis magnetostriction, dL_c/L_c , to 45 T at the base temperature of our measurements, 350 mK. At low fields, a broad feature is observed at $H_{MM} = 7.6$ T reminiscent of the AF1-AF3 transition discussed above (Fig. 1). Applying the known $1/\sin(\theta)$ dependence of this transition, we obtain that the actual angle between the c -axis and the magnetic field is $\theta = 17^\circ$. At higher fields, a small anomaly is buried in the background and the inset of Fig. 2 shows dL_c/L_c after the subtraction of a 4th order polynomial fit obtained in the range $15 < H < 29$ T. The subtracted data show a small lattice contraction at $H^* = 31$ T, $dL/L = -1.8 \times 10^{-6}$, in agreement with the upper limit of -2×10^{-6} obtained recently in pulsed fields [4]. Remarkably, there is no noticeable hysteresis in our data, which does not match the hysteretic resistivity obtained in thin microstructured samples, but agrees with virtually hysteresis-free resistivity curves obtained

in larger samples [22]. The lack of hysteresis along with a broader transition at H^* in bulk samples suggests that the nematic transition might actually be a crossover to a regime with large nematic susceptibility, which in turn is highly sensitive to strain. As elaborated in Ref. [22], the microstructured samples are coupled to the substrate, and the strain relaxation might be different in thinner samples. As a result, smaller samples may take longer to relax to equilibrium and hence may display hysteresis.

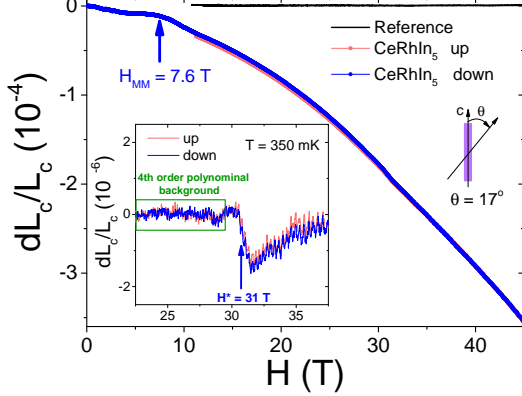


FIG. 2. Magnetostriction of CeRhIn₅ along the c -axis, dL_c/L_c , at $T = 350$ mK for fields applied 20° off the c -axis. Inset shows the data after a background subtraction.

The inset of Fig. 2 also shows sizable quantum oscillations at $H \gtrsim 27$ T. Although the presence of quantum oscillations (QO) in magnetostriction is a phenomenon known since the 60s [23], this is the first time magnetostriction QO are reported in CeRhIn₅, likely due to the fact that high-quality single crystals, high-resolution dilatometers, and low-noise environments (i.e. DC fields) are required. The amplitude of oscillations along the c -axis can be written as $-MH(\partial \ln A / \partial \sigma_c)$, where M is the amplitude of oscillations in magnetization, A is the extremal cross-sectional area of the FS perpendicular to the applied magnetic field, and σ_c is the stress along the c -axis. Therefore, magnetostriction QO provide information on the Fermi surface of materials, as do magnetization QO (i.e. dHvA), but the additional term $\partial \ln A / \partial \sigma_c$ enhances the amplitude of the stress-sensitive orbits. Here we will focus on the region $H > H^*$ because the QO amplitudes are larger above H^* , and our noise floor is higher in comparison to dHvA measurements [7].

Figure 3a shows the magnetostriction oscillations in inverse field and Figure 3b shows the corresponding FFT spectra at 350 mK. We observe four frequencies ($\alpha_3 = 3.7$ kT, $\alpha'_2 = 4.7$ kT, $\alpha'_1 = 5.7$ kT, and $\beta_2 = 6.2$ kT) which agree well with the frequencies obtained via dHvA for $30 < H < 45$ T at 330 mK and fields along the c -axis ($\alpha_3 = 3.7$ kT, $\alpha'_2 = 5$ kT, $\alpha'_1 = 5.7$ kT, and $\beta_2 = 6.3$ kT) [8]. We note that dHvA frequencies marked as α'_2 and α'_1 are observed only above H^* . By comparing the amplitude of the orbits given by the different techniques in similar conditions, one can obtain information on the strain dependence of the orbits. For instance, the β_2 amplitude is reduced in our data as compared to dHvA results

whereas the α'_2 is relatively enhanced. These results suggest that α'_2 orbit is a more strain-sensitive orbit than β_2 . We note, however, that this comparison should be taken with caution because magnetostriction and dHvA measurements were not performed on the same crystal and there may be differences in the FFT analysis performed in different experiments.

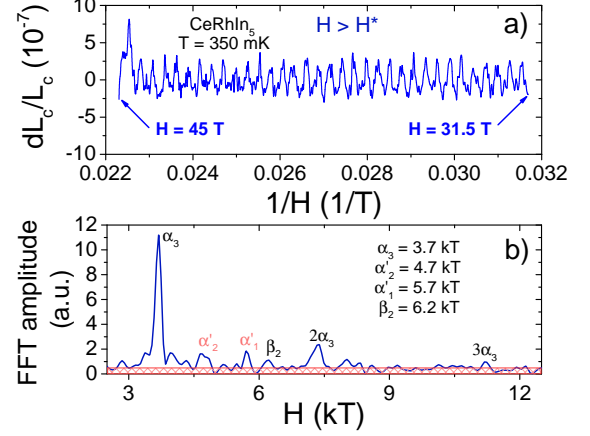


FIG. 3. a) Magnetostriction of CeRhIn₅ at 350 mK as a function of inverse field for fields applied $\simeq 20^\circ$ off the c -axis. For the sake of clarity, a high-pass filter was used to remove low-frequency oscillations that likely originate from the background difference below and above H^* . b) FFT spectra in the region $31.5 < H < 45$ T. The dashed area is an estimate of the noise floor.

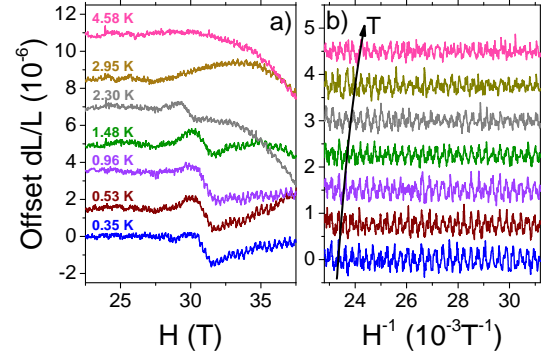


FIG. 4. a) Temperature dependence of the magnetostriction of CeRhIn₅ for fields applied $\simeq 20^\circ$ off the c -axis. An offset is added for the sake of clarity. b) High-field quantum oscillations in inverse field obtained from the data shown in panel a) after a high-pass filter is employed. The color scheme is the same as used in (a).

Figure 4a shows the c -axis magnetostriction at various temperatures for fields applied $\simeq 20^\circ$ off the c -axis. As the temperature increases, H^* remains fairly constant, but deviates to slightly lower fields at 2.3 K before vanishing at higher temperatures. We note that the anomaly at H^* detected in electrical resistance measurements becomes unobservable at $T > 2.2$ K, which could be a consequence of resolution limitations. By tracking H^* to higher temperatures, we are able to affirm that the nematic boundary most likely intercepts the AFM bound-

ary and disappears above T_N , as shown in the $H - T$ phase diagram to be discussed below (Fig. 5).

Figure 4b shows the high-field quantum oscillations in magnetostriction with increasing temperature. Although we are unable to reliably extract the T -dependence of the orbits α'_2 , α'_1 , and β_2 due to their small amplitudes, α_3 is significantly more intense and can be tracked to higher temperatures. Remarkably, the overall amplitude of the oscillations does not display the expected behavior for conventional metals within the Lifschitz-Kosevich (LK) formalism. According to the LK formula, the amplitude of the oscillations in a particular field range increases with decreasing temperature as $\propto m^*T/\sinh(Cm^*T)$, where C is a constant and m^* the effective mass [24]. Although the amplitude of the oscillations do decrease when comparing the temperature extremes (4.58 K and 0.35 K), there is no clear trend below 1 K. This is in agreement with dHvA measurements, both in pulsed and DC fields, that observe a decrease in the amplitude of the α_3 orbit below about 1 K [17, 25]. The interpretation of this anomalous behavior, however, is not settled. On one hand, the early report in pulsed fields attributes this decrease to the formation of spin-density-wave order [25]. On the other hand, more recent dHvA results in DC fields support a spin-dependent mass enhancement of the FS. In the latter, the QO amplitude is well described by a spin-dependent LK formula, suggesting a spin-split FS, as observed previously in CeCoIn₅ [17, 26]. In fact, we observe a beating pattern at frequencies close to α_3 , which could be taken as indicative of two Fermi pockets close together, one spin-up and one spin-down.

Finally, we discuss the implications of our results for the nature of the nematic phase. Figure 5 displays the H - T phase diagram of CeRhIn₅ with a compilation of recent high-field data. Because this phase diagram is constructed in the presence of a symmetry-breaking magnetic field, the phase boundary at H^* may be a crossover, instead of a true phase transition. In fact, removing the magnetic field does not seem to result in a residual resistivity anisotropy [4], which is indicative of a large nematic susceptibility, but no long-range nematic order.

If not long-range order, what changes at H^* that causes a large nematic susceptibility and why is the Kondo coupling robust in high magnetic fields? We recall that recent dHvA measurements reveal that the FS changes at H^* pointing to a larger FS in the nematic phase [7]. This indicates that the $4f$ electrons are being incorporated to the FS at H^* and are becoming more itinerant. Therefore, the main tuning parameter here must be the strength of the $4f$ -conduction electron hybridization. The key point therefore is that the hybridization depends on the Ce $4f$ ground-state wavefunction, which in turn is given by the crystal-field parameters in this particular tetragonal structure. Thus, the answer to our question lies in the field dependence of the wavefunctions determined by the crystalline electric field (CEF) and their anisotropic hybridization. For CeRhIn₅, the low-energy CEF levels are given by [27]:

$$\begin{aligned} |0\rangle &= \Gamma_7^2 = \alpha|\pm 5/2\rangle - \beta|\mp 3/2\rangle, \alpha = 0.62, \\ |1\rangle &= \Gamma_7^1 = \beta|\pm 5/2\rangle + \alpha|\mp 3/2\rangle, \beta = 0.78 \end{aligned} \quad (1)$$

where $|0\rangle$ is the ground state, $|1\rangle$ is the first-excited state at 7 meV, and α^2 determines the out-of-plane anisotropy. The pure $|5/2\rangle$ orbital is donut-shaped and hence higher α^2 corresponds to a more oblate $4f$ orbital confined to the ab -plane. Linear-polarized soft-x-ray absorption experiments reveal that the ground-state doublet changes from flatter (i.e. larger $|5/2\rangle$) orbitals in CeRhIn₅ to orbitals that are more extended along the c -axis in CeIrIn₅ and CeCoIn₅ (i.e. smaller $|5/2\rangle$) [28]. The prolate orbitals hybridize more strongly with out-of-plane In(2) electrons and, as a consequence, lead to superconducting ground states in CeIrIn₅ and CeCoIn₅.

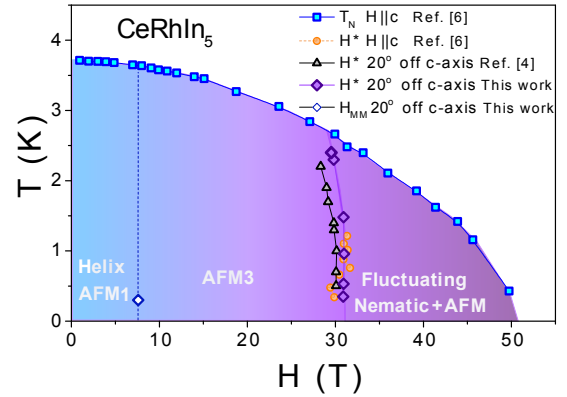


FIG. 5. $H - T$ phase diagram of CeRhIn₅. Data from Ref. [6] were obtained by specific heat measurements and Hall resistivity. Data from Ref. [4] were obtained by electrical resistivity measurements.

Now we can turn our attention to the field dependence of the orbitals in Eq. (1). Magnetic fields will, by the Zeeman effect, split the Γ_7 doublets and, therefore, promote mixing between the ground-state, Γ_7^2 , and the first-excited state, Γ_7^1 . Interestingly, the $|5/2\rangle$ contribution in the first excited state ($\beta = 0.78$) is larger than that of the original ground state ($\alpha = 0.62$), implying that the new, field-induced ground state wavefunction will become more confined to the basal plane. Because of its modified shape, the new ground state displays an enhanced hybridization with the in-plane In(1) electrons, similar to what happens with Sn-doped CeMIn₅ ($M = \text{Co, Rh}$) [29]. We note that this hybridization increase with In(1) electrons is fundamentally different from the hybridization with In(2) electrons observed in CeIrIn₅, CeCoIn₅, and likely CeRhIn₅ under pressure. This difference explains not only why the FS increases at H^* with the field-induced incorporation of $4f$ electrons, but it may also be the reason CeRhIn₅ is not superconducting as a function of field or Sn doping. Additionally, a similar crystal-field scenario has been used to explain recent nuclear magnetic resonance (NMR) experiments in high fields [30]. As a local probe, NMR is able to rule out a change in

the magnetic structure at H^* . Nevertheless, the fact that H^* develops only inside the magnetically ordered state along with the correlation between enhanced hybridization and enhanced nematic susceptibility suggests that the latter stems from the f -electron degrees of freedom. Whether a consequence of the frustration and the field-induced magnetic anisotropy in the spin degrees of freedom known to exist in CeRhIn₅ [11, 31] or a consequence of the hybridization gap remains an open question.

In summary, we performed high-resolution magnetostriiction measurements in CeRhIn₅ in DC fields to 45 T. At low fields, a finite in-plane field explicitly breaks the tetragonal (C_4) symmetry of the underlying lattice and reveals a small nematic susceptibility. At high fields, a small anomaly ($dL/L = -1.8 \times 10^{-6}$) in the c -axis magnetostriiction marks the onset of the nematic response at $H^* = 31$ T in CeRhIn₅ for fields $\simeq 20^\circ$ off the c -axis. The obtained $H - T$ phase diagram hosts a crossover line at H^* to a fluctuating nematic phase with high nematic susceptibility. This crossover occurs concomitantly to an enhancement in the Ce $4f$ hybridization with the in-plane In(1) conduction electrons, which explains why the Kondo coupling is robust in high fields. Our results also suggest that the nematic phase stems from the $4f$ degrees of freedom and their anisotropy translated to the

Fermi surface via hybridization. Therefore, the nematic behavior observed here in a prototypical heavy-fermion material is of electronic origin, and is driven by hybridization.

ACKNOWLEDGMENTS

We would like to acknowledge constructive discussions with P. G. Pagliuso, R. R. Urbano, L. Jiao, A. Severing, and E. Miranda. P. F. S. R. acknowledges support from the Laboratory Directed Research and Development program of Los Alamos National Laboratory under project number 20180618ECR. Sample synthesis was supported by the U.S. Department of Energy, Office of Basic Energy Sciences, Division of Materials Science and Engineering. M. J. acknowledges support from the Institute for Materials Science, LANL. A portion of this work was performed at the National High Magnetic Field Laboratory, which is supported by National Science Foundation Cooperative Agreement No. DMR-1157490 and the State of Florida. We thank J. B. Betts at the pulsed facility, and J. Billings and T. Murphy at the DC facility for their technical support. Theory work (RMF) was supported by the Office of Basic Energy Sciences, U.S. Department of Energy, under award DE-SC0012336.

-
- [1] J. Jensen and A. R. Mackintosh, *Rare Earth Magnetism*, Clarendon Press, Oxford (1991).
 - [2] P. Coleman, *Heavy Fermions: Electrons at the Edge of Magnetism*. Handbook of Magnetism and Advanced Magnetic Materials (2007).
 - [3] H von Lohneysen, A. Rosch, M. Votja, P. Wolfle, Rev. Mod Phys. **79**, 1015 (2007).
 - [4] F. Ronning, T. Helm, K. R. Shirer, M. D. Bachmann, L. Balicas, M. K. Chan, B. J. Ramshaw, R. D. McDonald, F. F. Balakirev, M. Jaime, E. D. Bauer, and P. J. W. Moll, Nature **548**, 313 (2017).
 - [5] E. Fradkin, S. A. Kivelson, M. J. Lawler, J. P. Eisenstein, and A. P. Mackenzie, Annu. Rev. Condens. Matter Phys. **1**, 153 (2010).
 - [6] R. M. Fernandes, A. V. Chubukov, and J. Schmalian, Nat. Phys. **10**, 97 (2014).
 - [7] L. Jiao, Y. Chen, Y. Kohama, D. Graf, E. D. Bauer, J. Singleton, Jian-Xin Zhu, Z. Weng, G. Pang, T. Shang, J. Zhang, Han-Oh Lee, T. Park, M. Jaime, J. D. Thompson, F. Steglich, Q. Si, and H. Q. Yuan, Proc. Natl. Acad. Sci. USA **112**, 673 (2014).
 - [8] L. Jiao, Z. F. Weng, M. Smidman, D. Graf, J. Singleton, E. D. Bauer, J. D. Thompson and H. Q. Yuan, Phil. Mag. **97**, 3446 (2017).
 - [9] W. Bao, P. G. Pagliuso, J. L. Sarrao, J. D. Thompson, Z. Fisk, J. W. Lynn, and R. W. Erwin, Phys. Rev. B **62**, R14621(R) (2000).
 - [10] D. M. Fobes, E. D. Bauer, J. D. Thompson, A. Sazonov, V. Hutanu, S. Zhang, F. Ronning, and M. Janoschek, J. Phys.: Condens. Matter **29** 17LT01 (2017).
 - [11] D. M. Fobes, S. Zhang, S.-Z. Lin, P. Das, N. J. Ghimire, E. D. Bauer, J. D. Thomson, L. W. Harriger, G. Ehlers, A. Podlesnyak, R. I. Bewley, A. Sazonov, V. Hutanu, F. Ronning, C. D. Batista, M. Janoschek, arXiv:1712.01761 (2017).
 - [12] H. Hegger *et al.*, Phys. Rev. Lett. **84**, 4986 (2000).
 - [13] T. Park, F. Ronning, H. Q. Yuan, M. B. Salamon, R. Movshovich, J. L. Sarrao and J. D. Thompson, Nature **440**, 65-68 (2006).
 - [14] T. Mito, S. Kawasaki, Y. Kawasaki, G. -q. Zheng, Y. Kitaoka, D. Aoki, Y. Haga, and Y. Onuki Phys. Rev. Lett. **90**, 077004 (2003).
 - [15] H. Shishido *et al*, J. Phys. Soc. Jpn. **71**, 162 (2002).
 - [16] L. Mendonça-Ferreira *et al*, Phys. Rev. Lett. **101**, 017005 (2008).
 - [17] L. Jiao, M. Smidman, Y. Kohama, Z. S. Wang, D. Graf, Z. F. Weng, Y. J. Zhang, A. Matsuo, E. D. Bauer, Hanoh Lee, S. Kirchner, J. Singleton, K. Kindo, J. Wosnitza, F. Steglich, J. D. Thompson, H. Q. Yuan, arXiv:1711.06191 (2017).
 - [18] G. M. Schmiedeshoff, A. W. Lounsbury, D. J. Luna, S. J. Tracy, A. J. Schramm, S. W. Tozer, V. F. Correa, S. T. Hannahs, T. P. Murphy, E. C. Palm, Rev. Sci. Instrum. **77**, 123907 (2006).
 - [19] M. Jaime *et al*, Sensors **17**, 2572 (2017).
 - [20] A. Ballato, IEEE Transactions on Ultrasonics, Ferroelectrics, and Frequency Control **43** (1995).
 - [21] R. S. Kumar *et al*, Phys. Rev. B **69**, 014515 (2004).
 - [22] P. J. W. Moll, B. Zeng, L. Balicas, S. Galeski, F. F. Balakirev, E. D. Bauer, and F. Ronning, Nat. Comm. **6**, 6663 (2015).
 - [23] B. A. Green, Jr. and B. S. Chandrasekhar, Phys. Rev.

- Lett. **11**, 331 (1963).
- [24] D. Shoenberg, Magnetic oscillations in metals (Cambridge University Press, 1984).
 - [25] A. L. Cornelius, A. J. Arko, J. L. Sarrao, M. F. Hundley, and Z. Fisk, Phys. Rev. B **62**, 14181 (2000).
 - [26] A. McCollam, S. R. Julian, P. M. C. Rourke, D. Aoki, and J. Flouquet, Phys. Rev. Lett. **94**, 186401 (2005).
 - [27] T. Willers, *et al*, Phys. Rev. B **81** 195114, (2010).
 - [28] T. Willers, *et al*, Proc. Natl. Acad. Sci. USA **112** 2384, (2015).
 - [29] K. Chen, *et al*, Phys. Rev. B **X Y**, (2017).
 - [30] G. G. Lesseux *et al*. Poster presentation, SCES meeting, Prague (2017).
 - [31] P. Das *et al.*, *Phys. Rev. Lett.* **113**, 246403 (2014).